THE JOURNAL OF PHYSICAL CHEMISTRY A
A JOURNAL OF THE AMERICAN CHEMICAL SOCIETY

pubs.acs.org/JPCA

Article

Atmospheric Oxidation of Hydroperoxy Amides

Eva R. Kjærgaard, Kristian H. Møller, and Henrik G. Kjaergaard*

Cite This: J. Phys. Chem. A 2023, 127, 9311−9321

Read Online

ACCESS | Metrics & More | Article Recommendations | Supporting Information

ABSTRACT: Recently, hydroperoxy amides were identified as major products of OH-initiated autoxidation of tertiary amines in the atmosphere. The formation mechanism is analogous to that found for ethers and sulfides but substantially faster. However, the atmospheric fate of the hydroperoxy amides remains unknown. Using high-level theoretical methods, we study the most likely OH-initiated oxidation pathways of the hydroperoxy and dihydroperoxy amides derived from trimethylamine autoxidation. Overall, we find that the OH-initiated oxidation of the hydroperoxy amides predominantly leads to the formation of imides under NO-dominated conditions and more highly oxidized hydroperoxy amides under HO_2-dominated conditions. Unimolecular reactions are found to be surprisingly slow, likely due to the restricting, planar structure of the amide moiety.

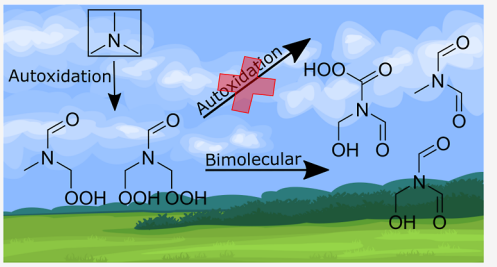

1. INTRODUCTION

Amines are emitted to the atmosphere from a range of sources including animal husbandry and biomass burning.[1] Methylamines (methylamine, dimethylamine, and trimethylamine) dominate the emissions and their combined annual emission is estimated to be 285 ± 78 Gg N.[1,2] Given the proposed use of amines for carbon capturing, atmospheric amine emissions may increase in the future.[3−5] Hence, the atmospheric oxidation of amines has received some attention, especially with a focus on bimolecular reactions and the formation of carcinogenic nitramines and nitrosamines.[4,6,7] However, it has recently been found that the peroxy radicals formed in the initial amine oxidation steps may instead react via fast unimolecular hydrogen shift (H-shift) reactions initiating autoxidation.[8−11] For the tertiary amines, this pathway is expected to dominate the oxidation under most atmospheric conditions.[8,10,11] For primary and secondary amines, the autoxidation pathway is limited by reactions preceding formation of the thermalized peroxy radicals.[4,7,8,12] One theoretical study[9] suggested that the autoxidation of tertiary amines may be hampered by decomposition reactions, but the significance of those pathways seems to be overestimated.[8,10,11]

The efficient autoxidation of amines was initially proposed by theory for trimethylamine (TMA) and was confirmed by free-jet flow experiments of the TMA + OH reaction in which functionalization of all three methyl groups was observed.[8] Recently, efficient autoxidation under atmospheric conditions has also been observed for triethylamine (TEA).[11] The previous combined theoretical and experimental results suggest that autoxidation is likely the dominant atmospheric oxidation pathway for tertiary amines under most atmospheric conditions.[8,10,11] The fast autoxidation suggests that hydroperoxy amides are the dominant products from TMA and TEA autoxidation, which is consistent with the molecular masses observed by chemical ionization mass spectrometry in the free-jet flow experiments.[8,10,11] This newly identified hydroperoxy amide product class is analogous to the ketohydroperoxides observed as key intermediates in for example low-temperature combustion of ethers and hydrocarbons.[13−18] For the ethers, the same products may be formed in the atmosphere via either autoxidation or Criegee intermediates reacting with carboxylic acids.[8,16,19,20]

Similarly, it has recently been found that autoxidation may account for 30−60% of the atmospheric oxidation of the important compound dimethyl sulfide (DMS) leading to the formation of the corresponding ketohydroperoxide known as hydroperoxymethyl thioformate (HPMTF).[21−25] This product has been observed experimentally during both flow cell and environmental chamber experiments.[22,25,26] Additionally, the NASA Atmospheric Tomography (ATom) campaigns 3 and 4 measured HPMTF as a ubiquitous sulfur compound in the global marine environment.[22,23] Under cloud-free conditions, reaction with OH is expected to dominate the atmospheric loss of HPMTF.[24,27] Theoretical results suggest that at room temperature, abstraction from the C**H**O group dominates followed by abstraction from the OO**H** group, while abstraction from the CH_2OOH group is a minor pathway.[21,25]

To the best of our knowledge, the atmospheric fate of the newly identified hydroperoxy amides has not been studied. As found for HPMTF and other small, highly oxidized compounds, important loss mechanisms may include hetero-

Received: July 5, 2023
Revised: September 22, 2023
Published: October 25, 2023

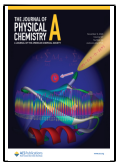

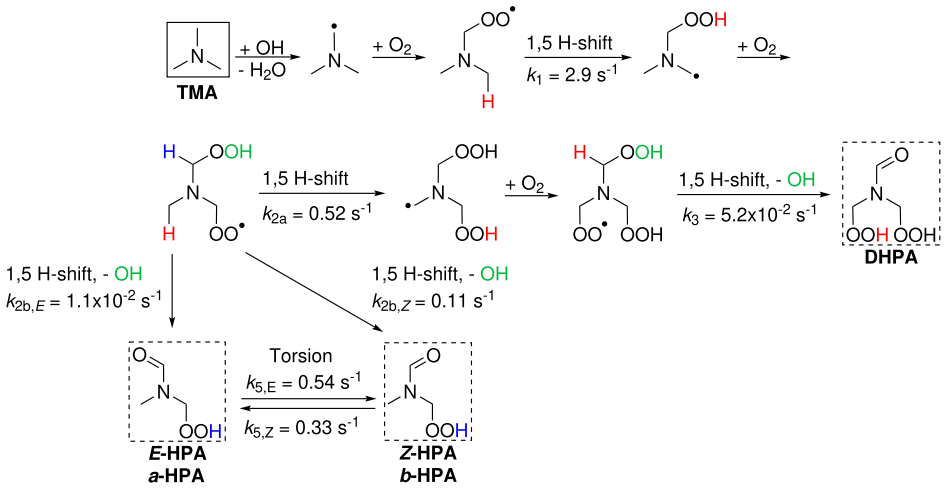

Figure 1. OH-initiated autoxidation of TMA leading to the formation of DHPA and the *E* and *Z* isomers of HPA. Rate coefficients of the unimolecular reactions are calculated using MC-TST at 298.15 K. The overall k_{2b} rate is 0.13 s^{-1} (Section S1).[8]

geneous uptake, photolysis, or reaction with atmospheric radicals of which OH is expected to dominate during daytime and NO_3 during nighttime.[4,28] The same mechanism of H-abstraction is expected for the reaction with OH, Cl, and NO_3, and the reaction with O_3 is expected to be negligible, as found for simple methyl amides.[28]

Here, we study the OH-initiated oxidation of the hydroperoxy amide and dihydroperoxy amide formed from trimethylamine autoxidation. For completeness, we study the subsequent reactions following abstraction of all unique hydrogen atoms in an attempt to form a complete mechanism leading to the next generation of closed-shell species.

2. METHODS

Reaction rate coefficients of the studied unimolecular reactions are calculated using the theoretical multiconformer transition state theory (MC-TST) approach for peroxy and alkoxy radical unimolecular reactions.[29,30] For a subset of the reactions, the final barrier height is calculated at a slightly lower level of ab initio theory. A brief description of the approach is given here.

Initially, an arbitrary conformer of reactant and transition state (TS) is optimized at the B3LYP/6-31+G(d) level (abbreviated B3LYP) using Gaussian 16.[31−36] Based on the optimized structures, a conformer search is performed using the Merck Mechanics Force Field (MMFF) in Spartan'18.[37,38] For the TS conformer searches, bond lengths of 3 bonds involved in the reactions are constrained. All conformer searches are carried out using a systematic 3-fold conformer search ("searchmethod = systematic") and keeping all identified conformers ("keepall"). For radical species, the additional keyword "ffhint=X∼∼+0" is used to specify the charge of the radical atom X to be 0.[29] All resulting conformers are optimized at the B3LYP level in Gaussian. For the TSs, a constrained optimization with the same constraints as those for the conformer sampling is performed first, followed by a free TS optimization. Frequency analyses are carried out to ensure that a minimum or first-order saddle point on the potential energy surface is located. Intrinsic reaction coordinate (IRC) calculations for the lowest-energy TS structure are done to validate the nature of each TS.

After the B3LYP optimizations, duplicate conformers are removed, by comparing their electronic energies and dipole moments.[29,39] All unique conformers (energies differing by more than 10^{-5} Hartree and dipole moments differing by more than 0.015 D) with electronic energies within 2 kcal/mol of the lowest-energy conformer are optimized at the ωB97X-D/aug-cc-pVTZ (abbreviated ωB97X-D) level.[40−42] The resulting energies and vibrational frequencies at this level are used to calculate the relative energies between conformers and their partition functions using the harmonic oscillator, rigid-rotor approximation. For the lowest-energy conformer of both reactant and TS, a spin-restricted open-shell CCSD(T)-F12a/VDZ-F12//ωB97X-D/aug-cc-pVTZ level (abbreviated CCSD(T)-F12a) single-point energy calculation is done using MOLPRO 2012.1 to obtain a more accurate barrier height.[43−48] This is done only for the initial reactions, while rate coefficients for the alkoxy reactions and subsequent reactions are calculated with barrier heights at the ωB97X-D/aug-cc-pVTZ level. This is expected to increase the uncertainty by about a factor of 10, which could affect which reaction pathway dominates some of the later oxidation steps. For competing reactions which share the reactant, the relative uncertainty is lower than the uncertainty in the MC-TST.[30,49] For the hydroperoxy H-shifts, the barrier heights are also calculated using ωB97X-D/aug-cc-pVTZ to avoid convergence issues previously encountered for these reactions and because they are fast enough that the absolute rates are less important.[50] As recommended with the VDZ-F12 basis set, the CCSD(T)-F12a calculations were done using gem_beta = 0.9.[47]

A tunneling coefficient is calculated using the asymmetrical one-dimensional Eckart approach.[51] Initially, an IRC calculation is performed on the B3LYP geometry of the TS conformer with the lowest zero-point corrected electronic energy at the ωB97X-D level. The IRC end points are optimized using first B3LYP followed by ωB97X-D. Finally, a single-point energy calculation is done at the CCSD(T)-F12a level. The Eckart tunneling factor is then calculated from barrier heights with CCSD(T)-F12a electronic energies and ωB97X-D zero-point corrections and the ωB97X-D imaginary TS frequency.

Finally, reaction rate coefficients, *k*, are calculated at 298.15 K using MC-TST:[29,52]

https://doi.org/10.1021/acs.jpca.3c04509
J. Phys. Chem. A 2023, 127, 9311−9321

$$k = \kappa \frac{k_B T}{h} \frac{\sum_i^{\text{TSconf.}} \exp\left(\frac{-\Delta E_i}{k_B T}\right) Q_{\text{TS}_i}}{\sum_j^{\text{Rconf.}} \exp\left(\frac{-\Delta E_j}{k_B T}\right) Q_{\text{R}_j}} \exp\left(-\frac{E_{\text{TS}} - E_{\text{R}}}{k_B T}\right) \quad (1)$$

κ is the Eckart tunneling coefficient, k_B is the Boltzmann constant, T is the temperature, h is Planck's constant, ΔE is the relative zero-point corrected energy of a given TS or reactant conformer, and Q is its partition function. $E_{TS} - E_R$ is the zero-point corrected energy difference between the lowest-energy TS and reactant conformers. The two sums are over all included TS and reactant conformers, respectively. MC-TST inherently calculates rate coefficients at the high-pressure limit. For fast alkoxy reactions, this has previously been found to lead to rate coefficients overestimated by up to a factor of 3 at atmospheric pressure.[30,53−56] For peroxy radical H-shifts, the deviation from the high-pressure limit has previously been found to be negligible at atmospheric pressure.[49,57−59]

For a few of the peroxy radical H-shifts, the rate coefficient of the reverse reaction was also calculated. In agreement with other systems previously studied in the literature, these reverse H-shifts are all found to be too slow to be of atmospheric importance (Table S10).[50,60] Thus, reverse peroxy radical H-shifts are generally not considered. Throughout this work, we have assumed O_2-addition to alkyl radicals to be barrierless and occur with a rate coefficient on the order of 10^{-11} cm^3 molecules^{-1} s^{-1}, in agreement with rate coefficients for amine-derived alkyl radicals in literature.[61]

Product yield distributions for different atmospheric lifetimes are modeled using Kintecus with unimolecular rate coefficients calculated here.[62] The reaction mechanisms are modeled at 298.15 K, with varying NO concentrations and a bimolecular NO rate coefficient of 8.73×10^{-12} molecules cm^{-3} s^{-1}. The initial peroxy radical distribution depends on which abstraction pathway is considered. The product concentrations at the final time point of 10^3 s were plotted as a function of NO concentration.

3. RESULTS AND DISCUSSION

As shown in Figure 1, the OH-initiated autoxidation of TMA leads to the formation of a hydroperoxy amide [HPA, *N*-(hydroperoxymethyl)-*N*-methylformamide)] and a dihydroperoxy amide [DHPA, *N*,*N*-bis(hydroperoxymethyl)-formamide]. In this autoxidation sequence, OH loss from the α-hydroperoxy alkyl radicals is assumed to be instantaneous, as previously found in the literature for comparable systems.[63,64] For most atmospheric conditions, the dihydroperoxy amide is expected to be the major product given the rate coefficients k_{2a} and k_{2b} of the two competing 1,5 H-shifts (Figure 1 and Table S1). The dominance of the dihydroperoxy amide and the corresponding peroxy radical over the hydroperoxy amide and peroxy radical has been observed in free-jet flow experiments.[10] As is typical for autoxidation, the H-shifts in this autoxidation sequence have previously been found to be highly temperature-dependent.[8,10,65] Analogous HPA and DHPA products were also found to dominate the OH oxidation in TEA.[11]

The previous studies identifying the atmospheric formation of the hydroperoxy amide HPA have considered it as a single product.[8−10] However, the N−CHO bond in the planar amides is known to exhibit a partial double bond character caused by resonance (Figure S1).[66] For interconversion between the two geometric isomers of HPA, we calculated torsional barriers of 14.6 and 15.7 kcal/mol, respectively, at the CCSD(T)-F12a level of theory. For comparison, experimentally determined torsional barriers for single bonds in simple organic molecules are a few kcal/mol.[67,68] The MC-TST rate coefficient for interconversion between *E*- and *Z*-HPA isomers is on the order of 0.5 s^{-1} (Figure 1). Where applicable, we consider the two geometric isomers, *E* and *Z*, separately. As the absolute *E*/*Z* configuration changes during oxidation, we use instead arbitrary labels *a* and *b* to distinguish between the two geometric isomers. Due to a slightly lower reaction barrier, the H-shift leading to *b*-HPA formation is faster than that leading to *a*-HPA formation by about a factor of 10 (Figure 1 and Table S1), and thus, initially, *b*-HPA will predominantly be formed. The total calculated rate of HPA formation (0.13 s^{-1}, Figure 1) is slightly different from the sum of the *Z*- and *E*-HPA formation pathways due to slight differences in the energies at different levels of theory and tunneling effects (Section S1). The total rate coefficient also differs slightly from the previously published value at the same level of theory due to the identification of an additional conformer here.[8] While *b*-HPA is formed much faster, the equilibrium abundances of the *a* and *b* isomers are more comparable, as reflected in the relative rate coefficients of their interconversion (Figure 1). Our modeling suggests that once formed, an equilibrium distribution between *b* and *a* of about 60:40 is reached in approximately 10 s (Figure S2).

Given the very recent identification of hydroperoxy amides as potentially important atmospheric species, no rate coefficients for their reaction with OH exist in the literature yet. Here, we will assume that HPA and DHPA react with OH with the same rate coefficient as the corresponding amide without the hydroperoxy group, *N*,*N*-dimethylformamide ($(CH_3)_2NCHO$), that is, $(1.4 \pm 0.3) \times 10^{-11}$ cm^3 molecule^{-1} s^{-1} at room temperature.[4,69] This assumption is based on experimentally inferred modeling for the analogous sulfur compound, HPMTF.[24,27] The assumed rate for HPA and DHPA with OH is in the typical range of rate coefficients for amides + OH, which spans $(0.35-2.15) \times 10^{-11}$ cm^3 molecules^{-1} s^{-1}.[4] This rate coefficient assumption is uncertain, but does not affect the mechanism, only the atmospheric lifetime of HPA and DHPA. With typical atmospheric OH concentrations of about 10^6 molecules cm^{-3}, the pseudo-first-order rate coefficient for the reaction of HPA and DHPA with OH is 1.4×10^{-5} s^{-1} corresponding to a lifetime for loss by OH of about 20 hours. Since the *a*/*b* equilibration is reached on timescales of seconds, these are expected to react with OH from their equilibrium distribution rather than the nascent distribution (Figure S2). Throughout this work, we will assume that the *a* and *b* isomers react bimolecularly with the same rate coefficients as calculation of these bimolecular rate coefficients with sufficient accuracy to reliably distinguish them is challenging and is expected to be of little overall importance for the conclusions of this manuscript. However, the unimolecular rate coefficients strongly depend on the distinction between *a* and *b* and are calculated for both isomers.

3.1. Initial Hydrogen Abstraction. HPA has four distinct hydrogen atoms that can be abstracted in the initial reaction with OH: −C**H**O, −C**H**$_3$, C**H**$_2$OOH, and −OO**H** (Figure 2). For *N*,*N*-dimethylformamide corresponding to HPA without the hydroperoxy group, abstraction from both the methyl groups and the carbonyl group has been observed.[12,28,69] For completeness, we include the subsequent reactions of all pathways. However, abstraction from the hydroperoxy

https://doi.org/10.1021/acs.jpca.3c04509
J. Phys. Chem. A 2023, 127, 9311−9321

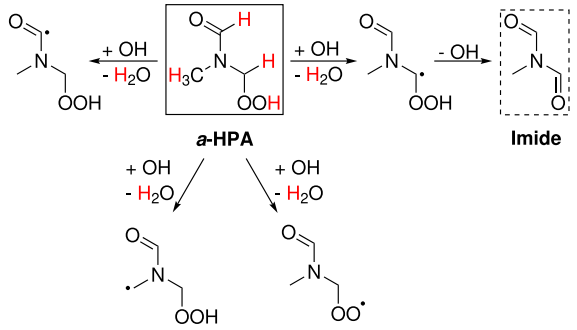

Figure 2. Pathways for H-abstraction by OH for *a*-HPA. The same pathways exist for *b*-HPA.

methylene group, is assumed to lead to prompt termination by loss of OH and formation of the imide, *N*-formyl-*N*-methylformamide (Figure 2) based on literature results for similar systems.[63,64] DHPA has only three different H-abstraction pathways, −C**H**O, −C**H**$_2$OOH, and −OO**H**, of which abstraction of the C**H**$_2$OOH hydrogen leads directly to termination by OH loss forming *N*-formyl-*N*-(hydroperoxymethyl)formamide (Figure S3).

3.2. DHPA Oxidation. *3.2.1. Hydroperoxy Hydrogen Abstraction.* Both calculations and experiments show that the dihydroperoxy amide is the dominant autoxidation product from TMA (Figure 1) and analogously for TEA under pristine atmospheric conditions.[8,10,11] As shown in Figure 3, abstraction of an H atom from either of the two hydroperoxy

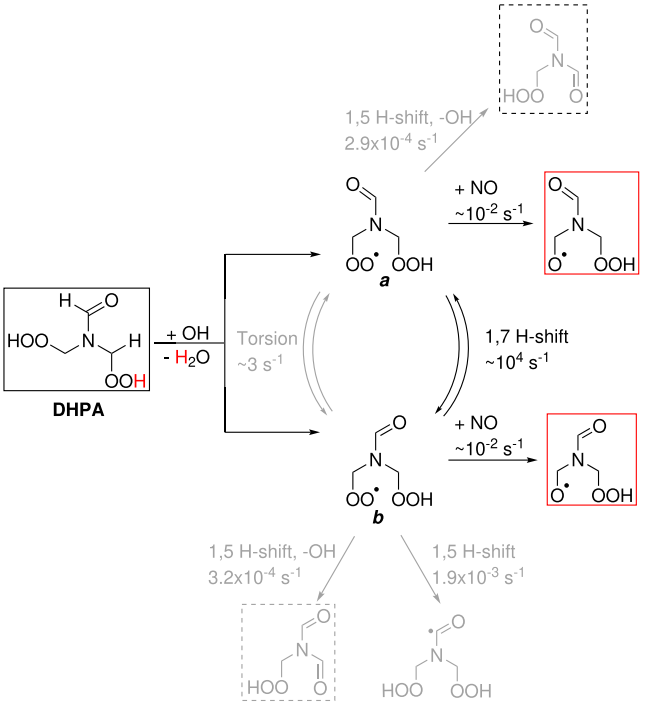

Figure 3. Initial oxidation steps following H-abstraction from either of the hydroperoxy groups in DHPA (black box). The expected major alkoxy radical intermediates are shown in red boxes, and minor closed-shell products are shown in dashed boxes. Rate coefficients of the unimolecular reactions are calculated using the MC-TST approach at 298.15 K. Less important pathways are shown in gray. Bimolecular rate coefficients of the peroxy radicals are estimated at lower-limit values based on the literature.

groups may form either the *a* or the *b* peroxy radical. These peroxy radicals may interconvert via either the torsion reaction with rate coefficients on the order of 3 s^{-1} or much faster via rapid OOH hydrogen shifts with rate coefficients on the order of 5 × 10^4 s^{-1} (Figure S4).[70−72] The latter reaction quickly leads to a steady-state peroxy radical distribution slightly favoring the *a*-peroxy radical.

The *a* and *b* peroxy radicals may react either bimolecularly with for example NO, HO_2, or RO_2 or unimolecularly via 1,5 H-shift reactions. For both peroxy radicals, we calculate the 1,5 H-shifts to be surprisingly slow (Figure 3) compared to similar 1,5 H-shifts in amines and hydrocarbons.[8,60] Thus, we expect both of the peroxy radicals to react bimolecularly, leading primarily to the hydroperoxy amide alkoxy radicals with a distribution determined by the relative stability of the two peroxy radicals, that is, favoring *a* (Figure S4).

The rate of the bimolecular peroxy radical reactions depends on the concentration of the reaction partners. The lower limit for the pseudo-first-order rate coefficient is on the order of 10^{-2} s^{-1} corresponding to pristine atmospheric conditions.[73−76] This corresponds to for example [NO] = 50 ppt with $k(RO_2 + NO) = 8.5 \times 10^{-12}$ cm^3 $molecule^{-1}$ s^{-1} or $[HO_2]$ = 20 ppt with $k(RO_2 + NO) = 2 \times 10^{-11}$ cm^3 $molecule^{-1}$ s^{-1}. Local NO concentrations may be lower than 50 ppt, but under such conditions, reactions with HO_2 or even RO_2 would still result in lower-limit peroxy radical pseudo-first-order rate coefficients of about 10^{-2} s^{-1}.[77−79] Under more polluted conditions, NO concentrations tend to be higher, increasing the overall pseudo-first-order rate coefficient of the bimolecular peroxy radical reactions and thus the importance of bimolecular reactions.[76] The reaction of the peroxy radicals with NO is expected to predominantly lead to the corresponding alkoxy radicals, with a small (∼5%) yield of the corresponding organonitrates.[10,75] The reaction with HO_2 is expected to predominantly form hydroperoxides rather than alkoxy radicals, terminating the radical propagation.[75,80] The reaction with other peroxy radicals, RO_2, may form alkoxy radicals, alcohols, aldehydes, or accretion products (ROOR), but is expected to have a minor overall importance. For simplicity, most reaction schemes throughout this work show only the bimolecular peroxy radical reactions with NO forming alkoxy radicals and a pseudo-first-order rate coefficient of 10^{-2} s^{-1}, representing a lower limit. The expected products under HO_2-dominated conditions are discussed in Section 3.5. In Figure 4, we illustrate the products and intermediates as a function of the bimolecular peroxy radical lifetime (exemplified by the NO concentration). The reaction mechanism is modeled in Kintecus[62] from the peroxy radicals with an initial 50:50 ratio of the *a*/*b* isomers assuming equal abstraction from either OOH group. The products and intermediates from the unimolecular reactions become important only for bimolecular lifetimes greater than about 100 s (Figure 4), but such long lifetimes are uncommon in the atmosphere.[76]

3.2.2. Carbonyl Hydrogen Abstraction. Abstraction of the carbonyl hydrogen (C**H**O) in DHPA forms an acyl radical (Figure 5). For comparable radicals formed from aldehydes, loss of CO tends to be fast and for HPMTF formed in DMS autoxidation, this pathway dominates following abstraction of the carbonyl H.[21,25,81] However, we calculate the CO loss reaction from this system to have an MC-TST rate coefficient of 5 × 10^{-5} s^{-1} and thus be completely negligible (Figure S5). The slow reaction is likely due to the partial double bond character of the C−N bond. Similarly, concerted loss of OH

https://doi.org/10.1021/acs.jpca.3c04509
J. Phys. Chem. A 2023, 127, 9311−9321

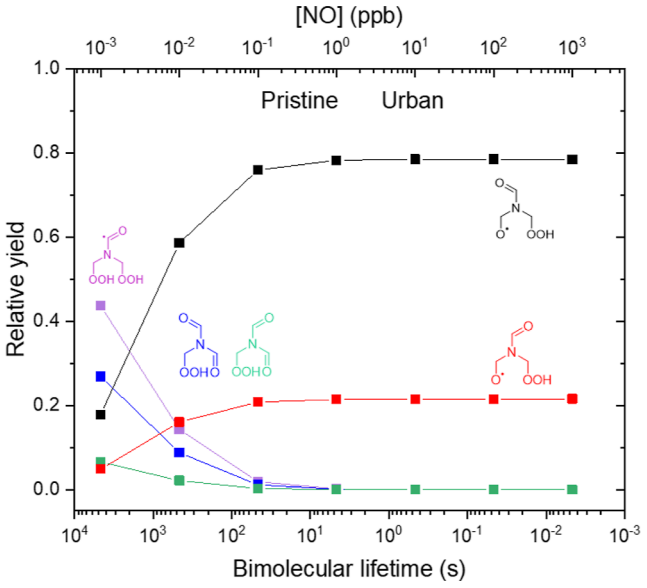

Figure 4. Relative yields of intermediates following H-abstraction from an OO**H** group in DHPA as a function of bimolecular lifetime of the peroxy radicals exemplified by reaction with NO. Modeled in Kintecus,[62] based on the mechanism presented in Figure 3. Typical pristine and urban conditions are indicated.[76]

and formaldehyde is calculated to be negligible, as is also found in the oxidation of HPMTF in the absence of excess energy.[21,25] Instead, the addition of molecular oxygen forms an acyl peroxy radical. As observed for hydrocarbon hydroperoxy acyl peroxy radicals in the literature, a H-shift abstracting the hydroperoxy hydrogen is fast and the equilibrium strongly favors the peroxy acid.[72] As found in the hydroperoxy H-abstraction pathway, the formed peroxy radical rapidly converts between the *a* and *b* isomers (Figure 3). Again, at lifetimes shorter than 100 s, both peroxy radicals react almost exclusively bimolecularly, in this case leading to the formation of hydroperoxy peroxy acid alkoxy radicals (Figure S6).

3.3. HPA Oxidation. The initial reactions following H-abstraction from HPA are largely analogous to those in DHPA but generally result in less oxidized alkoxy radicals given the less oxidized starting compound. As observed for DHPA, our calculations suggest that the only atmospherically competitive unimolecular peroxy radical reactions are H-shifts abstracting from hydroperoxy groups. Thus, the expected major initial intermediates are alkoxy radicals formed by bimolecular reactions of peroxy radicals with NO. The results are summarized in Figure 6, with details given in Section S3 for each of the abstraction pathways.

3.4. Alkoxy Radical Reactions. The initial steps following H-abstraction from DHPA and HPA (Figures 3, 5, and 6) are expected to primarily lead to two imides (formyl amides, nitrogen centers to which two carbonyl groups are bonded) and four unique amide-derived alkoxy radicals (Figure 7), each formed as some mixture of *a* and *b* (see Figures S13 and S14 for details). The alkoxy radicals have varying degrees of oxidation ranging from 2 to 6 oxygen atoms in total. In the atmosphere, alkoxy radicals typically react either unimolecularly by H-shifts or decomposition reactions or bimolecularly via H-abstraction by O_2 to form carbonyl compounds and HO_2. The rate of the bimolecular reaction with O_2 is relatively independent of the nature of the alkoxy radical, with pseudo-first-order rate coefficients on the order of 5×10^4 s^{-1} under typical atmospheric conditions.[82] This parametrization is based on results for alkyl alkoxy radicals and the rate coefficients may be different for species containing heteroatoms such as the ones studied here, introducing additional uncertainty.[83] The rate coefficients of the unimolecular reactions, on the other hand, depend strongly on the structure of the alkoxy radical.[82,84,85]

As for the peroxy radicals, we find that the different amide-derived alkoxy radicals follow similar reaction patterns. The possible reactions are illustrated in Figures 8 and 9 for A1 and A2, respectively, with mechanisms for A3 and A4, shown in

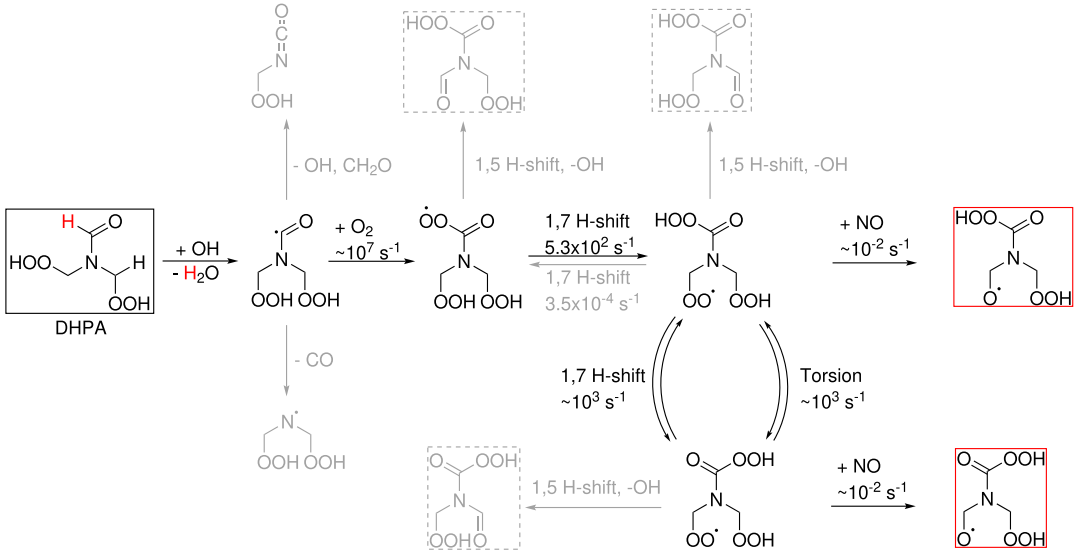

Figure 5. Oxidation mechanism following H-abstraction from the C**H**O group in DHPA (black box). Rate coefficients of the unimolecular reactions are calculated using the MC-TST approach at 298.15 K. The expected major alkoxy radical intermediates are shown in red boxes, and minor closed-shell products are shown in dashed boxes. Less important pathways are shown in gray. Bimolecular rate coefficients of the peroxy radicals are estimated lower-limit values based on the literature.

https://doi.org/10.1021/acs.jpca.3c04509
J. Phys. Chem. A 2023, 127, 9311−9321

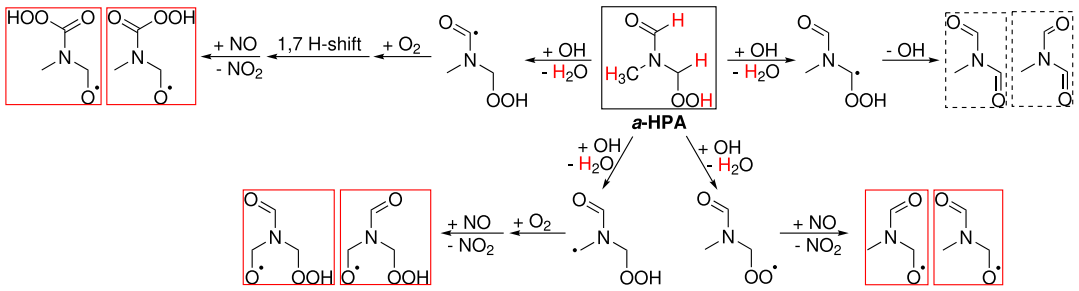

Figure 6. Summary of initial reactions following H-abstraction in HPA (black box). For simplicity, only *a*-HPA is shown, but the same reactions dominate for *b*-HPA. The expected major alkoxy radical intermediates are shown in red boxes, and closed-shell products are shown in dashed boxes.

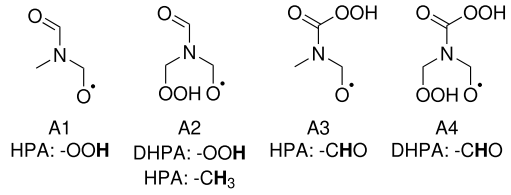

Figure 7. Overview of the dominant alkoxy radicals formed from the OH-initiated oxidation of HPA and DHPA. For the sake of simplicity, only the *a* isomer is shown for each. Below each radical, the H-abstraction pathway(s) leading to its formation is given.

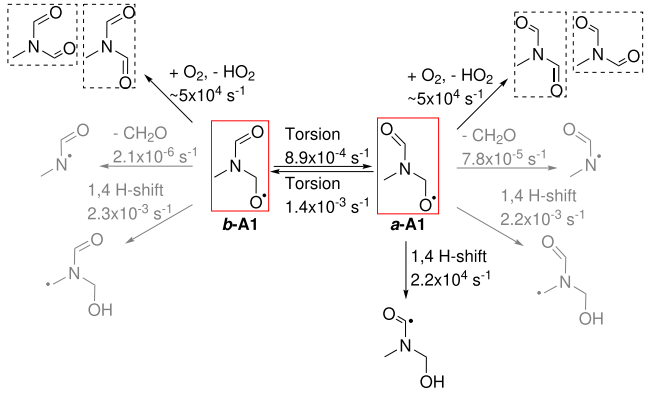

Figure 8. Reactions of alkoxy radical A1 (solid boxes) formed from the −OOH abstraction channel in HPA. Dominant imide products are shown in dashed boxes.

Section S5. For the largest alkoxy radical, A4, we do not calculate the rate coefficients of all reactions in the mechanism but infer the most likely outcome based on the results for the other three alkoxy radicals. For all alkoxy radicals, we find that their torsional interconversion rates are too slow to be atmospherically competitive and they thus retain their initial *a*/*b* distribution.

In Figure 8, we show the reaction pathway of the simplest of the formed alkoxy radicals, A1, which is formed from the abstraction of the hydroperoxy hydrogen in HPA followed by a bimolecular reaction (Figure 6). For both the *a* and *b* isomers of this alkoxy radical, we find that the 1,4 H-shift abstracting from the methyl group and the decomposition reactions are too slow to be of atmospheric importance. Relatively slow 1,4 alkoxy H-shifts are in agreement with findings for other systems in the literature.[85] However, for different carbon-based systems, the decomposition by loss of formaldehyde has been found to be fast ($k > 1\ s^{-1}$), as opposed to what is found here for these amide-derived systems.[82] This highlights a significant difference between the formation of a carbon-centered radical and an amide radical. The 1,4 H-shift abstracting the hydrogen from the carbonyl group is structurally possible only for the *a*-alkoxy radical for which it has an MC-TST rate coefficient of $2.2 \times 10^4\ s^{-1}$. This reaction is thus expected to be atmospherically competitive with the bimolecular reaction with O_2. However, from prior reaction steps (Section S3), the *b*-A1 radical is expected to be formed predominantly (>70%) suggesting that this pathway is unlikely to dominate the overall oxidation of A1. Speculation about the fate of this radical is given in Figure S18. The expected dominant reaction pathway for these alkoxy radicals is thus the bimolecular reaction with O_2, forming the three unique isomers of the imide *N*-formyl-*N*-methylformamide.

For the more highly oxidized alkoxy radicals, the oxidation pathways are more complex, as illustrated in Figure 9 for A2 formed from both HPA and DHPA (more complete reactions are shown in Figure S15). As observed previously for other systems, abstraction of a hydroperoxy hydrogen by an alkoxy radical is extremely fast with calculated MC-TST rate coefficients above $10^7\ s^{-1}$, outcompeting all other reactions.[10] Thus, the formation of the hydroxy amide peroxy radical is expected to be the sole fate of these alkoxy radicals. The newly formed peroxy radicals interconvert via torsion favoring the *b* isomer. Each of the peroxy radicals has a unimolecular reaction with a rate coefficient of about $10^{-3}\ s^{-1}$, which could represent a minor pathway. However, the reaction expected to dominate their reactivity is the bimolecular reaction with for example NO forming a new amide-derived hydroxy alkoxy radical. For the *b* alkoxy radical, the 1,4 H-shift abstracting from the carbonyl group is structurally available and this reaction may represent a minor atmospheric pathway, as found for the simpler alkoxy radical in Figure 8. However, again, the dominant route is expected to be reaction with O_2 to form the imide as a mix of *a* and *b* isomers.

The remaining two alkoxy radicals, A3 and A4 (Figure 7), react similarly to A1 and A2, respectively, also forming imides or substituted imides as the major products (Section S5). Unimolecular reactions involving the hydrogen on the hydroperoxy acid group are calculated not to matter.

3.5. Overall Oxidation Mechanism. We find that the rate coefficients of most unimolecular reactions in the oxidation of these hydroperoxy amides are too slow to be atmospherically important. This is in sharp contrast to the amines from which they are formed and for which the unimolecular peroxy radical H-shifts are found to be dominant.[8,10,11] The likely reason is that the planar structure imposed by the conjugation between the nitrogen and carbonyl group leads to large strain in the TS, increasing its energy and thus the reaction barrier. The

https://doi.org/10.1021/acs.jpca.3c04509
J. Phys. Chem. A 2023, 127, 9311−9321

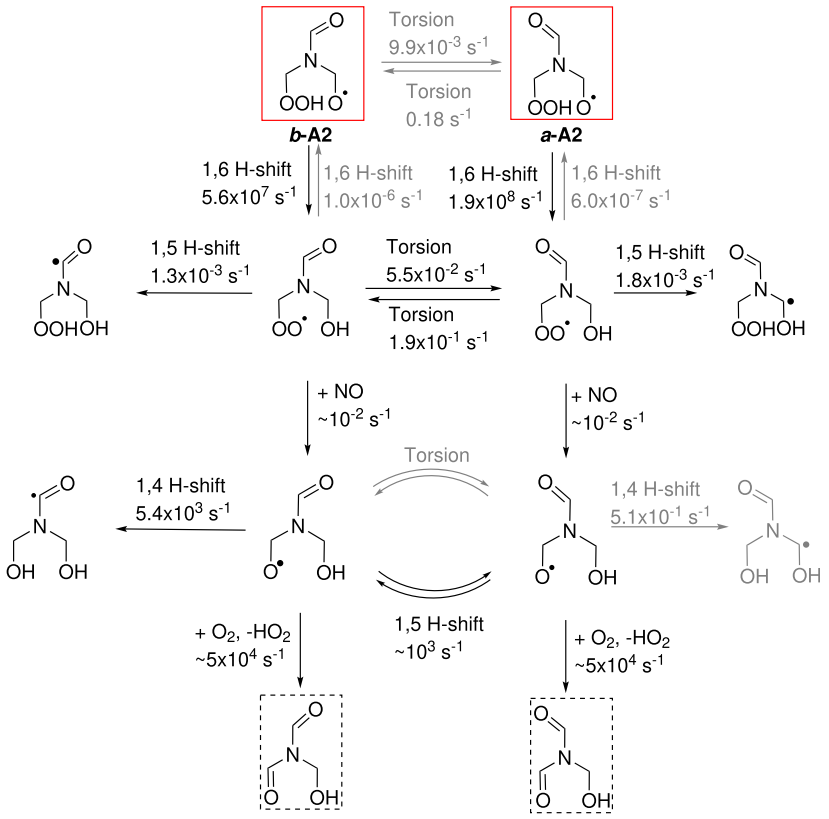

Figure 9. Selected alkoxy reactions of alkoxy radical A2 (solid boxes) formed from both HPA (CH_3 abstraction) and DHPA (OOH abstraction). Dominant imide products are shown in dashed boxes. Less important pathways are shown in gray. Bimolecular rate coefficients of the peroxy radicals are estimated lower-limit values based on the literature.

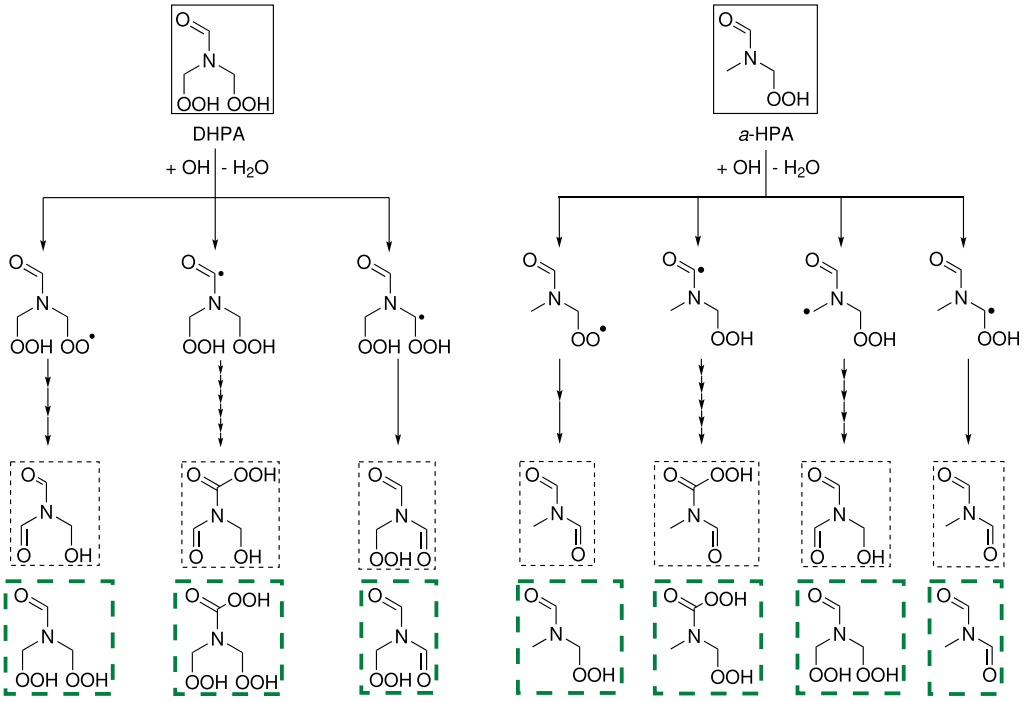

Figure 10. Overview of the dominant products formed from the OH-initiated oxidation of HPA and DHPA when the bimolecular reactions of the peroxy radicals are dominated by NO (first row, black dashed boxes) or HO_2 (second row, green dashed boxes). The products from abstraction of the CH_2OOH hydrogen are the same in both cases as this mechanism does not involve a bimolecular reaction step following the initial H-abstraction by OH. The number of arrows represents the minimum number of reaction steps required to reach the product shown. For simplicity, only the *a*-isomers are shown.

https://doi.org/10.1021/acs.jpca.3c04509
J. Phys. Chem. A 2023, 127, 9311−9321

exceptions to the slow unimolecular reactions in these amides are reactions which are generally very fast in other, less-constrained systems: hydroperoxy H-shifts from hydroperoxy groups and alkoxy H-shifts from hydroxy, hydroperoxy, or aldehyde groups.[10,49,71] Most of these reactions remain fast enough to maintain their atmospheric importance for the systems studied here.

The dominant reaction pathways are governed by bimolecular reactions. Overall, the OH-initiated oxidation of HPA and DHPA under conditions dominated by bimolecular reactions with NO is found to lead to the formation of a range of different imides with up to two hydroxy or hydroperoxy groups (Figure 10). The simplest of the proposed imide products, *N*-formyl-*N*-methyl formamide, which is formed from OO**H** and C**H**$_2$OOH abstraction in HPA under NO-dominated conditions has been determined experimentally to be the dominant product (∼70%) in the OH-initiated oxidation of *N*,*N*-dimethylformamide identical to HPA without the hydroperoxy group.[28] The proposed dominant reactions in *N*,*N*-dimethylformamide are analogous to the reaction pathways proposed to dominate here but without the added complexity from the hydroperoxy groups, in support of the mechanisms identified here.

However, the products of the atmospheric oxidation depend on the dominant bimolecular reaction partners of the peroxy radicals formed.[79,80] Under pristine conditions where bimolecular reactions of the peroxy radicals with HO_2 dominate over reactions with NO, a new set of hydroperoxy amides rather than imides are expected to be the dominant products (Section S6 and Figure 10). This bifurcation is as expected from the known atmospheric chemistry of NO and HO_2.[79,80]

As is typical for the competition between NO and HO_2 as bimolecular reaction partners, the products under HO_2-dominated conditions are more highly oxidized (higher O/C ratios). Additionally, they have hydroperoxy groups, as opposed to hydroxy groups and formyl groups. Hydroperoxy groups have been shown to form stronger hydrogen bonds than hydroxy groups.[86] Thus, the products under HO_2-dominated conditions are expected to have lower volatilities and are likely more susceptible to aerosol uptake. HPA itself has an O/C ratio of 1, while DHPA has an O/C ratio of 1.67. Compared to HPA and DHPA themselves, the product pool under NO-dominated conditions is largely comparable to or less oxidized, while the product pool under HO_2-dominated conditions is generally at least as highly oxidized as HPA and DHPA. Assuming that the products in Figure 10 are formed in comparable amounts, the average O/C ratios under NO-dominated conditions are 0.92 and 1.33 for the HPA and DHPA oxidation products, respectively. Under HO_2-dominated conditions, the corresponding O/C ratios are 1.25 and 1.78, respectively.

The distribution between the different products under a given set of conditions will largely depend on the initial site of H-abstraction, which should be investigated further, optimally by experimental means. The nascent *a*/*b* distribution of the formed products will further depend on the concentrations of bimolecular reaction partners in the different oxidation steps affecting the viability of the torsion reactions. However, as found for HPA (Figure S2), it is likely that the isomers of the closed-shell products (Figure 10) will reach a steady state before further reaction in the atmosphere.

The existing experimental work on TMA oxidation observing autoxidation and the formation of HPA and DHPA is performed on timescales of less than 8 s.[8,10] Attempts at increasing the OH concentration to accelerate this process and observe subsequent OH reaction, lead instead to the formation of hydrotrioxides.[87] As such, chamber experiments on the OH-initiated oxidation of TMA over long timescales are likely necessary to assess the proposed oxidation mechanisms and possibly extract the branching ratios for the different pathways. Additionally, studies of the atmospheric properties of these proposed new products would be necessary to evaluate their atmospheric impacts and possible degradation pathways. Given their high degree of functionalization, uptake into clouds or aerosol particles may represent an important atmospheric loss pathway of HPA and DHPA, which should be studied further.[88]

4. CONCLUSIONS

The atmospheric autoxidation of tertiary amines quickly forms hydroperoxy amides in large yields. Using multiconformer transition state theory, we study the oxidation pathways of the hydroperoxy and dihydroperoxy amides that are formed in the autoxidation of TMA. We find that given the partial double bond character of the amide group, the different geometric isomers (*E*/*Z*) need to be considered separately but they may interconvert. Additionally, the partial double bond constrains the structure and thus significantly slows the unimolecular H-shift reactions in the amides. Their oxidation mechanism is thus governed by bimolecular reactions, in contrast to the amines from which they are derived. Under high-NO conditions, the dominant products are expected to be imides (formyl amides) formed via alkoxy pathways. Under more pristine conditions characterized by bimolecular HO_2 reactions, the dominant products are instead expected to be more highly oxidized hydroperoxy amides.

■ ASSOCIATED CONTENT

Data Availability Statement

Output-files from the ωB97X-D/aug-cc-pVTZ and CCSD(T)-F12a/cc-pVDZ-F12 calculations including energies, partition functions, and the optimized ωB97X-D/aug-cc-pVTZ geometries are available online at: https://erda.ku.dk/archives/de4f7be1614779daa47184a77c620126/published-archive.html.

Supporting Information

The Supporting Information is available free of charge at https://pubs.acs.org/doi/10.1021/acs.jpca.3c04509.

Formation rates, initial oxidation steps, products and intermediates formed, alkoxy reactions, HO_2-dominated conditions, and rate coefficient calculation parameters (PDF)

■ AUTHOR INFORMATION

Corresponding Author

Henrik G. Kjaergaard − *Department of Chemistry, University of Copenhagen, DK-2100 Copenhagen Ø, Denmark;* orcid.org/0000-0002-7275-8297; Email: hgk@chem.ku.dk

Authors

Eva R. Kjærgaard − *Department of Chemistry, University of Copenhagen, DK-2100 Copenhagen Ø, Denmark;* Present Address: Department of Chemistry, Aarhus University,

https://doi.org/10.1021/acs.jpca.3c04509
J. Phys. Chem. A 2023, 127, 9311−9321

Langelandsgade 140, 8000 Aarhus C, Denmark; orcid.org/0000-0001-8838-0084

Kristian H. Møller − *Department of Chemistry, University of Copenhagen, DK-2100 Copenhagen Ø, Denmark;* Present Address: The Danish Meteorological Institute, Lyngbyvej 100, DK-2100 Copenhagen Ø, Denmark.; orcid.org/0000-0001-8070-8516

Complete contact information is available at: https://pubs.acs.org/10.1021/acs.jpca.3c04509

Notes

The authors declare no competing financial interest.

■ ACKNOWLEDGMENTS

We thank Jing Chen and Nanna Falk Christensen for their helpful discussions. This work was supported by funding from the Novo Nordisk Foundation Interdisciplinary Synergy Program (NNF19OC0057374) and VILLUM FONDEN (VIL50443), and computer time was provided by the High Performance Computing Centre at the University of Copenhagen.

■ REFERENCES

(1) Ge, X.; Wexler, A. S.; Clegg, S. L. Atmospheric Amines − Part I. A Review. *Atmos. Environ.* **2011**, *45*, 524−546.

(2) Schade, G. W.; Crutzen, P. J. Emission of Aliphatic Amines from Animal Husbandry and Their Reactions: Potential Source of N_2O and HCN. *J. Atmos. Chem.* **1995**, *22*, 319−346.

(3) Fostås, B.; Gangstad, A.; Nenseter, B.; Pedersen, S.; Sjøvoll, M.; Sørensen, A. L. Effects of NO_x in the Flue Gas Degradation of MEA. *Energy Procedia* **2011**, *4*, 1566−1573.

(4) Nielsen, C. J.; Herrmann, H.; Weller, C. Atmospheric Chemistry and Environmental Impact of the Use of Amines in Carbon Capture and Storage (CCS). *Chem. Soc. Rev.* **2012**, *41*, 6684−6704.

(5) Zhu, L.; Schade, G. W.; Nielsen, C. J. Real-Time Monitoring of Emissions from Monoethanolamine-Based Industrial Scale Carbon Capture Facilities. *Environ. Sci. Technol.* **2013**, *47*, 14306−14314.

(6) Murphy, S. M.; Sorooshian, A.; Kroll, J. H.; Ng, N. L.; Chhabra, P.; Tong, C.; Surratt, J. D.; Knipping, E.; Flagan, R. C.; Seinfeld, J. H. Secondary Aerosol Formation from Atmospheric Reactions of Aliphatic Amines. *Atmos. Chem. Phys.* **2007**, *7*, 2313−2337.

(7) Onel, L.; Blitz, M.; Dryden, M.; Thonger, L.; Seakins, P. Branching Ratios in Reactions of OH Radicals with Methylamine, Dimethylamine, and Ethylamine. *Environ. Sci. Technol.* **2014**, *48*, 9935−9942.

(8) Møller, K. H.; Berndt, T.; Kjaergaard, H. G. Atmospheric Autoxidation of Amines. *Environ. Sci. Technol.* **2020**, *54*, 11087−11099.

(9) Ma, F.; Xie, H.-B.; Li, M.; Wang, S.; Zhang, R.; Chen, J. Autoxidation Mechanism for Atmospheric Oxidation of Tertiary Amines: Implications for Secondary Organic Aerosol Formation. *Chemosphere* **2021**, *273*, 129207.

(10) Berndt, T.; Møller, K. H.; Herrmann, H.; Kjaergaard, H. G. Trimethylamine Outruns Terpenes and Aromatics in Atmospheric Autoxidation. *J. Phys. Chem. A* **2021**, *125*, 4454−4466.

(11) Kjærgaard, E. R.; Møller, K. H.; Berndt, T.; Kjaergaard, H. G. Highly Efficient Autoxidation of Triethylamine. *J. Phys. Chem. A* **2023**, *127*, 8623−8632.

(12) Nielsen, C.; D'Anna, B.; Karl, M.; Aursnes, M.; Boreave, A.; Bossi, R.; Bunkan, A.; Glasius, M.; Hallquist, M.; Hansen, A.-M.; et al. *Atmospheric Degradation of Amines (ADA) Summary Report: Photo-Oxidation of Methylamine*, Dimethylamine and Trimethylamine CLIMIT project no. 201604, 2011.

(13) Jenkin, M. E.; Hayman, G. D.; Wallington, T. J.; Hurley, M. D.; Ball, J. C.; Nielsen, O. J.; Ellermann, T. Kinetic and Mechanistic Study of the Self-Reaction of Methoxymethylperoxy Radicals at Room Temperature. *J. Phys. Chem.* **1993**, *97*, 11712−11723.

(14) Curran, H.; Gaffuri, P.; Pitz, W.; Westbrook, C. A Comprehensive Modeling Study of n-Heptane Oxidation. *Combust. Flame* **1998**, *114*, 149−177.

(15) Moshammer, K.; Jasper, A. W.; Popolan-Vaida, D. M.; Lucassen, A.; Diévart, P.; Selim, H.; Eskola, A. J.; Taatjes, C. A.; Leone, S. R.; Sarathy, S. M.; et al. Detection and Identification of the Keto-Hydroperoxide ($HOOCH_2OCHO$) and Other Intermediates during Low-Temperature Oxidation of Dimethyl Ether. *J. Phys. Chem. A* **2015**, *119*, 7361−7374.

(16) Wang, S.; Wang, L. The Atmospheric Oxidation of Dimethyl, Diethyl, and Diisopropyl Ethers. The Role of the Intramolecular Hydrogen Shift in Peroxy Radicals. *Phys. Chem. Chem. Phys.* **2016**, *18*, 7707−7714.

(17) Moshammer, K.; Jasper, A. W.; Popolan-Vaida, D. M.; Wang, Z.; Bhavani Shankar, V. S.; Ruwe, L.; Taatjes, C. A.; Dagaut, P.; Hansen, N. Quantification of the Keto-Hydroperoxide ($HOOCH_2OCHO$) and Other Elusive Intermediates during Low-Temperature Oxidation of Dimethyl Ether. *J. Phys. Chem. A* **2016**, *120*, 7890−7901.

(18) Wang, Z.; Herbinet, O.; Hansen, N.; Battin-Leclerc, F. Exploring Hydroperoxides in Combustion: History, Recent Advances and Perspectives. *Prog. Energy Combust. Sci.* **2019**, *73*, 132−181.

(19) Porterfield, J. P.; Lee, K. L. K.; Dell'Isola, V.; Carroll, P. B.; McCarthy, M. C. Characterization of the Simplest Hydroperoxide Ester, Hydroperoxymethyl Formate, a Precursor of Atmospheric Aerosols. *Phys. Chem. Chem. Phys.* **2019**, *21*, 18065−18070.

(20) Cabezas, C.; Endo, Y. Observation of Hydroperoxyethyl Formate from the Reaction Between the Methyl Criegee Intermediate and Formic Acid. *Phys. Chem. Chem. Phys.* **2020**, *22*, 446−454.

(21) Wu, R.; Wang, S.; Wang, L. New Mechanism for the Atmospheric Oxidation of Dimethyl Sulfide. The Importance of Intramolecular Hydrogen Shift in a CH_3SCH_2OO Radical. *J. Phys. Chem. A* **2015**, *119*, 112−117.

(22) Berndt, T.; Scholz, W.; Mentler, B.; Fischer, L.; Hoffmann, E. H.; Tilgner, A.; Hyttinen, N.; Prisle, N. L.; Hansel, A.; Herrmann, H. Fast Peroxy Radical Isomerization and OH Recycling in the Reaction of OH Radicals with Dimethyl Sulfide. *J. Phys. Chem. Lett.* **2019**, *10*, 6478−6483.

(23) Veres, P. R.; Neuman, J. A.; Bertram, T. H.; Assaf, E.; Wolfe, G. M.; Williamson, C. J.; Weinzierl, B.; Tilmes, S.; Thompson, C. R.; Thames, A. B.; et al. Global Airborne Sampling Reveals a Previously Unobserved Dimethyl Sulfide Oxidation Mechanism in the Marine Atmosphere. *Proc. Natl. Acad. Sci. U.S.A.* **2020**, *117*, 4505−4510.

(24) Novak, G. A.; Fite, C. H.; Holmes, C. D.; Veres, P. R.; Neuman, J. A.; Faloona, I.; Thornton, J. A.; Wolfe, G. M.; Vermeuel, M. P.; Jernigan, C. M.; et al. Rapid Cloud Removal of Dimethyl Sulfide Oxidation Products Limits SO_2 and Cloud Condensation Nuclei Production in the Marine Atmosphere. *Proc. Natl. Acad. Sci. U.S.A.* **2021**, *118*, No. e2110472118.

(25) Jernigan, C. M.; Fite, C. H.; Vereecken, L.; Berkelhammer, M. B.; Rollins, A. W.; Rickly, P. S.; Novelli, A.; Taraborrelli, D.; Holmes, C. D.; Bertram, T. H. Efficient Production of Carbonyl Sulfide in the Low-NOx Oxidation of Dimethyl Sulfide. *Geophys. Res. Lett.* **2022**, *49*, No. e2021GL096838.

(26) Ye, Q.; Goss, M. B.; Isaacman-VanWertz, G.; Zaytsev, A.; Massoli, P.; Lim, C.; Croteau, P.; Canagaratna, M.; Knopf, D. A.; Keutsch, F. N.; et al. Organic Sulfur Products and Peroxy Radical Isomerization in the OH Oxidation of Dimethyl Sulfide. *ACS Earth Space Chem.* **2021**, *5*, 2013−2020.

(27) Vermeuel, M. P.; Novak, G. A.; Jernigan, C. M.; Bertram, T. H. Diel Profile of Hydroperoxymethyl Thioformate: Evidence for Surface Deposition and Multiphase Chemistry. *Environ. Sci. Technol.* **2020**, *54*, 12521−12529.

(28) Barnes, I.; Solignac, G.; Mellouki, A.; Becker, K. H. Aspects of the Atmospheric Chemistry of Amides. *ChemPhysChem* **2010**, *11*, 3844−3857.

(29) Møller, K. H.; Otkjær, R. V.; Hyttinen, N.; Kurtén, T.; Kjaergaard, H. G. Cost-Effective Implementation of Multiconformer Transition State Theory for Peroxy Radical Hydrogen Shift Reactions. *J. Phys. Chem. A* **2016**, *120*, 10072−10087.
(30) Zhao, Q.; Møller, K. H.; Chen, J.; Kjaergaard, H. G. Cost-Effective Implementation of Multiconformer Transition State Theory for Alkoxy Radical Unimolecular Reactions. *J. Phys. Chem. A* **2022**, *126*, 6483−6494.
(31) Becke, A. D. Density-Functional Thermochemistry. III. The Role of Exact Exchange. *J. Chem. Phys.* **1993**, *98*, 5648−5652.
(32) Lee, C.; Yang, W.; Parr, R. G. Development of the Colle-Salvetti Correlation-Energy Formula into a Functional of the Electron Density. *Phys. Rev. B* **1988**, *37*, 785−789.
(33) Hehre, W. J.; Ditchfield, R.; Pople, J. A. Self-Consistent Molecular Orbital Methods. XII. Further Extensions of Gaussian-Type Basis Sets for Use in Molecular Orbital Studies of Organic Molecules. *J. Chem. Phys.* **1972**, *56*, 2257−2261.
(34) Clark, T.; Chandrasekhar, J.; Spitznagel, G. W.; Schleyer, P. V. R. Efficient Diffuse Function-augmented Basis Sets for Anion Calculations. III. The 3-21+G Basis Set for First-row Elements, Li−F. *J. Comput. Chem.* **1983**, *4*, 294−301.
(35) Frisch, M. J.; Pople, J. A.; Binkley, J. S. Self-consistent molecular orbital methods 25. Supplementary functions for Gaussian basis sets Supplementary Functions for Gaussian Basis Sets. *J. Chem. Phys.* **1984**, *80*, 3265−3269.
(36) Frisch, M. J.; Trucks, G. W.; Schlegel, H. B.; Scuseria, G. E.; Robb, M. A.; Cheeseman, J. R.; Scalmani, G.; Barone, V.; Petersson, G. A.; Nakatsuji, H.; et al. *Gaussian 16*, Revision C.01; Gaussian Inc: Wallingford CT, 2016.
(37) Halgren, T. A. Merck Molecular Force Field. I. Basis, Form, Scope, Parameterization, and Performance of MMFF94. *J. Comput. Chem.* **1996**, *17*, 490−519.
(38) *Spartan'18*; Wavefunction Inc.: Irvine, CA, 1996.
(39) Otkjær, R. V.; Møller, K. H. Removal of Duplicate Conformers. 1996, https://github.com/TheKjaergaardGroup/Removal-of-Duplicate-Conformerwebs.
(40) Chai, J.-D.; Head-Gordon, M. Long-range Corrected Hybrid Density Functionals with Damped Atom-atom Dispersion Corrections. *Phys. Chem. Chem. Phys.* **2008**, *10*, 6615−6620.
(41) Dunning, T. H. Gaussian Basis Sets for Use in Correlated Molecular Calculations. I. The Atoms Boron Through Neon and Hydrogen. *J. Chem. Phys.* **1989**, *90*, 1007−1023.
(42) Kendall, R. A.; Dunning, T. H.; Harrison, R. Electron affinities of the first-row atoms revisited. Systematic basis sets and wave functions. *J. Chem. Phys.* **1992**, *96*, 6796−6806.
(43) Watts, J. D.; Gauss, J.; Bartlett, R. J. Coupled-cluster Methods with Noniterative Triple Excitations for Restricted Open-shell Hartree-Fock and Other General Single Determinant Reference Functions. Energies and Analytical Gradients. *J. Chem. Phys.* **1993**, *98*, 8718−8733.
(44) Adler, T. B.; Knizia, G.; Werner, H.-J. A Simple and Efficient CCSD(T)-F12 Approximation. *J. Chem. Phys.* **2007**, *127*, 221106.
(45) Knizia, G.; Adler, T. B.; Werner, H.-J. Simplified CCSD(T)-F12 Methods: Theory and Benchmarks. *J. Chem. Phys.* **2009**, *130*, 054104.
(46) Werner, H.-J.; Knizia, G.; Manby, F. R. Explicitly Correlated Coupled Cluster Methods with Pair-specific Geminals. *Mol. Phys.* **2011**, *109*, 407−417.
(47) Peterson, K. A.; Adler, T. B.; Werner, H.-J. Systematically Convergent Basis Sets for Explicitly Correlated Wavefunctions: The Atoms H, He, B−Ne, and Al−Ar. *J. Chem. Phys.* **2008**, *128*, 084102.
(48) Werner, H.-J.; Knowles, P. J.; Knizia, G.; Manby, F. R.; Schütz, M.; Celani, P.; Györffy, W.; Kats, D.; Korona, T.; Lindh, R.; et al. *MOLPRO, version 2012.1, a Package of Ab Initio Programs*. 2012, http://www.molpro.newebt.
(49) Møller, K. H.; Bates, K. H.; Kjaergaard, H. G. The Importance of Peroxy Radical Hydrogen-Shift Reactions in Atmospheric Isoprene Oxidation. *J. Phys. Chem. A* **2019**, *123*, 920−932.
(50) Praske, E.; Otkjær, R. V.; Crounse, J. D.; Hethcox, J. C.; Stoltz, B. M.; Kjaergaard, H. G.; Wennberg, P. O. Intramolecular Hydrogen Shift Chemistry of Hydroperoxy-Substituted Peroxy Radicals. *J. Phys. Chem. A* **2019**, *123*, 590−600.
(51) Eckart, C. The Penetration of a Potential Barrier by Electrons. *Phys. Rev.* **1930**, *35*, 1303−1309.
(52) Vereecken, L.; Peeters, J. The 1,5-H-shift in 1-Butoxy: A Case Study in the Rigorous Implementation of Transition State Theory for a Multirotamer System. *J. Chem. Phys.* **2003**, *119*, 5159−5170.
(53) Méreau, R.; Rayez, M.-T.; Caralp, F.; Rayez, J.-C. Theoretical study of alkoxyl radical decomposition reactions: structure−activity relationships. *Phys. Chem. Chem. Phys.* **2000**, *2*, 3765−3772.
(54) Somnitz, H.; Zellner, R. Theoretical studies of unimolecular reactions of C2−C5 alkoxy radicals. Part II. RRKM dynamical calculations. *Phys. Chem. Chem. Phys.* **2000**, *2*, 1907−1918.
(55) Méreau, R.; Rayez, M.-T.; Caralp, F.; Rayez, J.-C. Isomerisation reactions of alkoxy radicals: theoretical study and structure−activity relationships. *Phys. Chem. Chem. Phys.* **2003**, *5*, 4828−4833.
(56) Somnitz, H. The contribution of tunnelling to the 1,5 H-shift isomerisation reaction of alkoxyl radicals. *Phys. Chem. Chem. Phys.* **2008**, *10*, 965−973.
(57) Peeters, J.; Müller, J. F.; Stavrakou, T.; Nguyen, V. S. Hydroxyl Radical Recycling in Isoprene Oxidation Driven by Hydrogen Bonding and Hydrogen Tunneling: The Upgraded LIM1Mechanism. *J. Phys. Chem. A* **2014**, *118*, 8625−8643.
(58) Miyoshi, A. Molecular size dependent falloff rate constants for the recombination reactions of alkyl radicals with O2 and implications for simplified kinetics of alkylperoxy radicals. *Int. J. Chem. Kin.* **2012**, *44*, 59−74.
(59) Xing, L.; Bao, J. L.; Wang, Z.; Wang, X.; Truhlar, D. G. Hydrogen shift isomerizations in the kinetics of the second oxidation mechanism of alkane combustion. Reactions of the hydroperoxypentylperoxy OOQOOH radical. *Combust. Flame* **2018**, *197*, 88−101.
(60) Otkjær, R. V.; Jakobsen, H. H.; Tram, C. M.; Kjaergaard, H. G. Calculated Hydrogen Shift Rate Constants in Substituted Alkyl Peroxy Radicals. *J. Phys. Chem. A* **2018**, *122*, 8665−8673.
(61) Rissanen, M. P.; Eskola, A. J.; Nguyen, T. L.; Barker, J. R.; Liu, J.; Liu, J.; Halme, E.; Timonen, R. S. $CH_2NH_2 + O_2$ and $CH_3CHNH_2 + O_2$ Reaction Kinetics: Photoionization Mass Spectrometry Experiments and Master Equation Calculations. *J. Phys. Chem. A* **2014**, *118*, 2176−2186.
(62) Ianni, J. C. *Kintecus, Windows version 6.01*. 1996, www.kintecus.cowebm.
(63) Vereecken, L.; Nguyen, T.; Hermans, I.; Peeters, J. Computational study of the stability of α-hydroperoxyl- or α-alkylperoxyl substituted alkyl radicals. *Chem. Phys. Lett.* **2004**, *393*, 432−436.
(64) Anglada, J. M.; Crehuet, R.; Francisco, J. S. The Stability of α-Hydroperoxyalkyl Radicals. *Chem.—Eur. J.* **2016**, *22*, 18092−18100.
(65) Praske, E.; Otkjær, R. V.; Crounse, J. D.; Hethcox, J. C.; Stoltz, B. M.; Kjaergaard, H. G.; Wennberg, P. O. Atmospheric Autoxidation is Increasingly Important in Urban and Suburban North America. *Proc. Natl. Acad. Sci. U.S.A.* **2018**, *115*, 64−69.
(66) Pauling, L.; University, C.; Press, C. U. The Nature of the Chemical Bond and the Structure of Molecules and Crystals. In *An Introduction to Modern Structural Chemistry*; George Fisher Baker Non-Resident Lecture Series; Cornell University Press, 1960.
(67) Durig, J. R.; Feng, F. S.; Wang, A.; Phan, H. V. Conformational Stability, Barriers to Internal Rotation, Ab Initio Calculations, and Vibrational Assignment of 2-butanone. *Can. J. Chem.* **1991**, *69*, 1827−1844.
(68) NIST Computational Chemistry Comparison and Benchmark Database. NIST Standard Reference Database Number 101 1996.
(69) Solignac, G.; Mellouki, A.; Le Bras, G.; Barnes, I.; Benter, T. Kinetics of the OH and Cl reactions with N-methylformamide, N,N-dimethylformamide and N,N-dimethylacetamide. *J. Photochem. Photobiol., A* **2005**, *176*, 136−142.
(70) Miyoshi, A. Systematic Computational Study on the Unimolecular Reactions of Alkylperoxy (RO_2), Hydroperoxyalkyl

https://doi.org/10.1021/acs.jpca.3c04509
J. Phys. Chem. A 2023, 127, 9311−9321

(QOOH), and Hydroperoxyalkylperoxy (O_2QOOH) Radicals. *J. Phys. Chem. A* **2011**, *115*, 3301−3325.
(71) Jørgensen, S.; Knap, H. C.; Otkjær, R. V.; Jensen, A. M.; Kjeldsen, M. L. H.; Wennberg, P. O.; Kjaergaard, H. G. Rapid Hydrogen Shift Scrambling in Hydroperoxy-Substituted Organic Peroxy Radicals. *J. Phys. Chem. A* **2016**, *120*, 266−275.
(72) Knap, H. C.; Jørgensen, S. Rapid Hydrogen Shift Reactions in Acyl Peroxy Radicals. *J. Phys. Chem. A* **2017**, *121*, 1470−1479.
(73) Mao, J.; Ren, X.; Zhang, L.; Van Duin, D. M.; Cohen, R. C.; Park, J.-H.; Goldstein, A. H.; Paulot, F.; Beaver, M. R.; Crounse, J. D.; et al. Insights into Hydroxyl Measurements and Atmospheric Oxidation in a California Forest. *Atmos. Chem. Phys.* **2012**, *12*, 8009−8020.
(74) Lelieveld, J.; Butler, T. M.; Crowley, J. N.; Dillon, T. J.; Fischer, H.; Ganzeveld, L.; Harder, H.; Lawrence, M. G.; Martinez, M.; Taraborrelli, D.; et al. Atmospheric Oxidation Capacity Sustained by a Tropical Forest. *Nature* **2008**, *452*, 737−740.
(75) Wennberg, P. O.; Bates, K. H.; Crounse, J. D.; Dodson, L. G.; McVay, R. C.; Mertens, L. A.; Nguyen, T. B.; Praske, E.; Schwantes, R. H.; Smarte, M. D.; et al. Gas-Phase Reactions of Isoprene and Its Major Oxidation Products. *Chem. Rev.* **2018**, *118*, 3337−3390.
(76) Bianchi, F.; Kurtén, T.; Riva, M.; Mohr, C.; Rissanen, M. P.; Roldin, P.; Berndt, T.; Crounse, J. D.; Wennberg, P. O.; Mentel, T. F.; et al. Highly Oxygenated Organic Molecules (HOM) from Gas-Phase Autoxidation Involving Peroxy Radicals: A Key Contributor to Atmospheric Aerosol. *Chem. Rev.* **2019**, *119*, 3472−3509.
(77) Emmons, L.; Carroll, M.; Hauglustaine, D.; Brasseur, G.; Atherton, C.; Penner, J.; Sillman, S.; Levy, H.; Rohrer, F.; Wauben, W.; et al. Climatologies of NO_xx and NO_y: A comparison of data and models. *Atmos. Environ.* **1997**, *31*, 1851−1904.
(78) Day, D. A.; Farmer, D. K.; Goldstein, A. H.; Wooldridge, P. J.; Minejima, C.; Cohen, R. C. Observations of NO_x, ΣPNs, ΣANs, and HNO_3 at a Rural Site in the California Sierra Nevada Mountains: summertime diurnal cycles. *Atmos. Chem. Phys.* **2009**, *9*, 4879−4896.
(79) Chen, J.; Møller, K. H.; Wennberg, P. O.; Kjaergaard, H. G. Unimolecular Reactions Following Indoor and Outdoor Limonene Ozonolysis. *J. Phys. Chem. A* **2021**, *125*, 669−680.
(80) Orlando, J. J.; Tyndall, G. S. Laboratory Studies of Organic Peroxy Radical Chemistry: An Overview with Emphasis on Recent Issues of Atmospheric Significance. *Chem. Soc. Rev.* **2012**, *41*, 6294−6317.
(81) Méreau, R.; Rayez, M.-T.; Rayez, J.-C.; Caralp, F.; Lesclaux, R. Theoretical Study on the Atmospheric Fate of Carbonyl Radicals: Kinetics of Decomposition Reactions. *Phys. Chem. Chem. Phys.* **2001**, *3*, 4712−4717.
(82) Atkinson, R. Rate Constants for the Atmospheric Reactions of Alkoxy Radicals: An Updated Estimation Method. *Atmos. Environ.* **2007**, *41*, 8468−8485.
(83) Dibble, T. S.; Chai, J. *Advances in Atmospheric Chemistry*; World Scientific, 2017; Chapter 3, pp 185−269.
(84) Vereecken, L.; Peeters, J. Decomposition of Substituted Alkoxy Radicals—Part I: A Generalized Structure−Activity Relationship for Reaction Barrier Heights. *Phys. Chem. Chem. Phys.* **2009**, *11*, 9062−9074.
(85) Vereecken, L.; Peeters, J. A Structure−Activity Relationship for the Rate Coefficient of H-migration in Substituted Alkoxy Radicals. *Phys. Chem. Chem. Phys.* **2010**, *12*, 12608−12620.
(86) Møller, K. H.; Tram, C. M.; Kjaergaard, H. G. Side-by-Side Comparison of Hydroperoxide and Corresponding Alcohol as Hydrogen-Bond Donors. *J. Phys. Chem. A* **2017**, *121*, 2951−2959.
(87) Berndt, T.; Chen, J.; Kjærgaard, E. R.; Møller, K. H.; Tilgner, A.; Hoffmann, E. H.; Herrmann, H.; Crounse, J. D.; Wennberg, P. O.; Kjaergaard, H. G. Hydrotrioxide (ROOOH) formation in the atmosphere. *Science* **2022**, *376*, 979−982.
(88) Burkholder, J. B.; Sander, S. P.; Abbatt, J.; Barker, J. R.; Cappa, C.; Crounse, J. D.; Dibble, T. S.; Huie, R. E.; Kolb, C. E.; Kurylo, M. J.; et al. *Chemical Kinetics and Photochemical Data for Use in Atmospheric Studies*. Evaluation No. 19, 2019.

https://doi.org/10.1021/acs.jpca.3c04509
J. Phys. Chem. A 2023, 127, 9311−9321